AIAA SciTech Forum
7-11 January 2019, San Diego, California
AIAA Scitech 2019 Forum

10.2514/6.2019-1584

Conceptual Design of a Co-Flow Jet Hybrid Electric Regional Airliner

Yunchao Yang * Gecheng Zha †
Dept. of Mechanical and Aerospace Engineering
University of Miami, Coral Gables, Florida 33124
E-mail: gzha@miami.edu

Abstract

The Co-Flow Jet (CFJ) flow control technology is promising to radically improve the takeoff/landing and cruise performance of aircraft due to its substantial lift augmentation and drag reduction performance with very low energy expenditure. A new promising technology in aircraft design is hybrid electric propulsion (HEP) technology, which integrates fuel engines and batteries to improve the energy efficiency and reduce CO_2 emissions. The CFJ technology intrinsically employs distributed electric propulsion and is a desirable option for HEP.

This paper investigates the potential benefits of Co-Flow jet (CFJ) hybrid electric propulsion (HEP) aircraft through a conceptual design of a regional airliner. The ATR72-500 regional airliner is chosen as the baseline for reference. The ATR72-500 aircraft has a range of 890 nm, a payload of 72 passengers and cruise Mach number of 0.46. The mission of the current CFJ hybrid electric regional airliner (CFJ-HERA) is to extend the range of ATR72-500. The CFJ-HERA uses an optimized CFJ wing configuration based on the CFJ6421-SST150-INJ117-SUC247 airfoil. Two different aspect ratios of 12 and 20 are studied for comparison. Both achieve substantially higher productivity efficiency than the baseline ATR72-500 airliner. With the same wing area as that of ATR72-500, the CFJ-HERA-AR12 design achieves a substantially longer range of 1960 nm and the CFJ-HERA-AR20 further extends the range to 2850 nm. Due to the high lift cruise coefficient of a CFJ wing, the CFJ-HERA has a wing loading of 660 kg/m^2 and 746 kg/m^2 for AR of 12 and 20 respectively. In addition to the increased productivity efficiency, the significantly higher wing loading allows the airliner to carry much more fuel and batteries without increasing the wing size and weight, which contributes to the substantially longer range. The conceptual design of the CFJ-HERA indicates that the CFJ technology has a great potential to contribute the development of hybrid propulsion aircraft.

1 Overview

1.1 Hybrid Electric Propulsion

To combat the global warming and reduce emissions, the electric-based propulsion has attracted more and more interests in the aviation industry [1]. Full electric propulsion (FEP) relies on batteries as the sole energy source. Hybrid electric propulsion (HEP) is a fusion of combustion and electric propulsion system. It may or may not use batteries as the sole energy source.

The advantages of fully electric/hybrid electric propulsion techniques include less carbon and NOx emissions, lower noise, and higher efficiency, etc. However, the full electric propulsion is currently constrained by its lower energy and power density, which requires aircraft to carry a large amount of battery and thus limits the range. The hybrid propulsion still uses combustions engines, which can operate at its optimum operating conditions. At the

* Ph.D. , AIAA student member
† Professor, AIAA associate Fellow

same time, electric motors work efficiently in a wide operating range. Since the total power output depends on the combined power of the combustion engine and electric motors, the maximum power required for the combustion engine is reduced (e.g. maximum power for takeoff). Therefore, the energy conversion efficiency of the hybrid engine is higher than that of a conventional engine, which has to sacrifice the efficiency to trade for a broad operating range of a whole flight envelope.

The other important advantage of an electric-based propulsion system is that it can be straightforwardly incorporated with a distributed electric propulsion (DEP), which can be implemented by a spanwise distribution of multiple propulsion units along the wing/fuselage. The electric power from the fuel engines can be transited to the multiple propulsion units, such as motors and fans with small energy loss by electric cables. The power generator and the propulsors can be placed on desirable locations on the vehicle to optimize overall system performance [2]. The overall reduced fuel consumption due to higher system efficiency and decreased weight of the core combustion engines of HEP can offset the weight increase due to the added motors and generators.

Despite their great potentials, the development of fully electric and hybrid electric propulsion in aviation is still in its embryonic stage. This paper is to make an effort to enhance the efficiency of a hybrid regional airliner by using the recently developed Co-flow Jet (CFJ) active flow control technology, which is promising to achieve high wing loading and aerodynamic efficiency at cruise and ultra-high lift coefficient at takeoff/landing.

1.2 Co-Flow Jet Flow Control

The concept of CFJ flow control airfoil developed by Zha et al. [3, 4, 5, 6, 7, 8, 9, 10, 11, 12, 13, 14, 15, 16, 17, 18] achieves a dramatically lift augmentation, drag reduction and stall margin increase at low energy expenditure. It can not only achieve ESTOL performance with ultra-high maximum lift coefficient, but also significantly enhance cruise efficiency and cruise lift coefficient (wing loading) from subsonic to transonic conditions [10, 11, 12, 13].

The CFJ airfoil has an injection slot near the leading edge (LE) and a suction slot near the trailing edge (TE) on the airfoil upper surface as sketched in Fig. 1. A small amount of mass flow is withdrawn into the airfoil near the TE, pressurized and energized by a pumping system inside the airfoil, and then injected near the LE in the direction tangent to the main flow. The entire process does not add any mass flow to the system and hence is a zero-net mass-flux (ZNMF) flow control. It is a self-contained high lift system with no moving parts.

The fundamental mechanism of the CFJ airfoil is that the turbulent mixing between the jet and main flow energizes the wall boundary-layer, which dramatically increases the circulation, augmenting lift, and reducing the total drag(or generates thrust) by filling the wake velocity deficit. The CFJ airfoil has a unique low energy expenditure mechanism because the jet gets injected at the leading edge suction peak location, where the main flow pressure is the lowest and makes it easy to eject the flow, and it gets sucked at near the trailing edge, where the main flow pressure is the highest and makes it easy to withdraw the flow.

Yang and Zha [13] indicate that CFJ airfoil is able to achieve Super-Lift coefficient (SLC) at takeoff/landing and high cruise efficiency at cruise. It is beneficial to have larger injection slot size for high cruise efficiency, whereas to achieve Super-Lift coefficient for takeoff/landing, a reduced injection slot size with higher jet speed is more desirable. Fig. 2 is the flow structures of a super-lift coefficient CFJ airfoil flow at AoA=70° from 2D RANS simulation [13]. A very high circulation generating the super-lift coefficient makes the stagnation point detached from the airfoil. The trailing edge vortex creates an extended virtual solid body to form a high-pressure region due to the stagnant flow to support the airfoil with super-lift coefficient. The high-momentum jet mixes with the free stream and makes the flow attached on the suction surface.

The wind tunnel experiment investigation of the CFJ airfoil [18] is conducted in the subsonic wind tunnel at

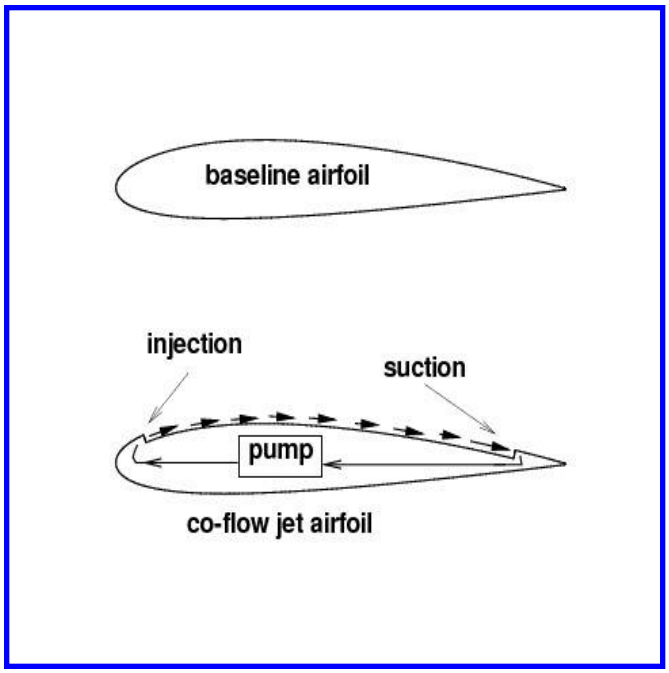

Figure 1: Baseline airfoil and CFJ airfoil.

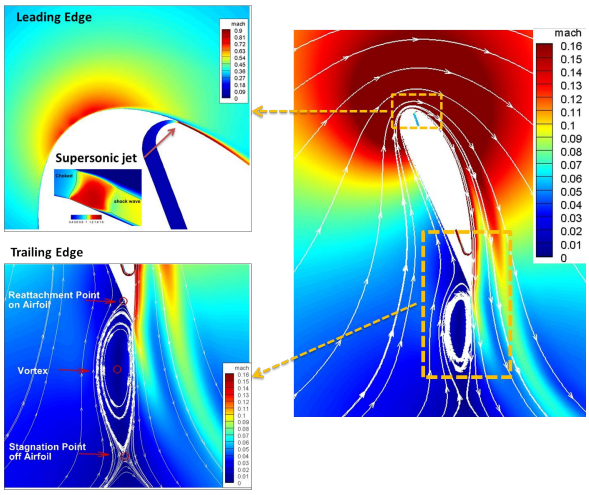

Figure 2: Mach number contours and streamlines at $C_\mu = 0.35$ and AoA =70° for the CFJ6421-SST016-SUC053-INJ009 airfoil. [13]

Texas A&M University. The experimental study prove the super-lift coefficient of CFJ6421 airfoil. The C_{Lmax} achieved in the experiment varies from 8.0 to 8.6, substantially exceeding the theoretical limit of 7.6. The CFJ airfoil is also able to generate a very high thrust coefficient. Both the high lift and thrust are attributed to the super-suction effect with very low pressure at the airfoil leading edge induced by the injection jet.

1.3 Potential Benefits of CFJ Hybrid Electric Propulsion Aircraft

The following potential benefits are identified for CFJ aircraft:

- The CFJ wings generates super lift coefficient for Extremely Short Takeoff/Landing (ESTOL) performance and low community noise.
- Reduce fuel consumption and emission pollution by the high cruise efficiency of the CFJ wings.
- Reduce wing and control surface size and weight due to high lift coefficient .
- Elimination of aircraft control surfaces through differential and vectoring thrust of CFJ;
- CFJ wings comprise the distributed propulsion system intrinsically integrated with the airframe to improve aircraft system efficiency by reducing wake mixing loss.
- High safety and reliability due to redundancy of multiple micro-compressors.

There is a growing demand for regional airline market recently. The hybrid electric propulsion regional airliners appeal to industry for their high efficiency, low noise, and low emission pollution, such as the E-Fan X co-developed by Airbus, Rolls-Royce, and Siemens. The objective of this paper is to conduct a conceptual design of a CFJ

regional airliner with hybrid electric propulsion as an example to demonstrate the advantage of CFJ-HEP aircraft. The CFJ wing serves as a crucial part of the high-efficiency aircraft with hybrid electric distributed propulsion.

2 Conceptual Design of Hybrid Electric Propulsion Aircraft

2.1 Hybrid Electric Propulsion

The hybrid electric propulsion is defined as the power and energy storage combined by the conventional fuel and electric components. Two major types of hybrid strategies are commonly applied: series and parallel. In the series hybrid configuration, the chemical energy in jet fuel is converted to the electricity to charge the battery or to drive the motor. The series drivetrain is considered as the simplest configuration. The combustion engine can be downsized because power demands requirement for the engine is reduced. Moreover, the electrical power is more easily distributed to multiple fans/propulsors for the purpose of distributed propulsion. For demonstration purpose in this study, the series hybrid drivetrain is selected to design the CFJ distributed electric propulsion aircraft.

2.2 Range Equation for Series Hybrid Electric Propulsion

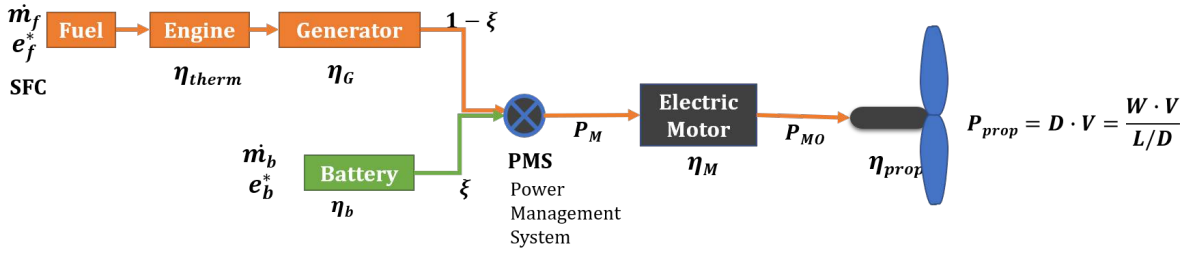

E_{total} : Total installed energy, (kWh)		η_{therm} : Efficiency of the combustion engine;	
E_b : Battery installed energy, (kWh)		η_b : Battery charging and discharging efficiency;	
m_b : Battery weight, (kg)		η_M : Efficiency of the electric motor;	
m_f : Fuel weight, (kg)		η_{prop} : Propeller efficiency;	
e_b^* : Battery Specific energy, (kWh/kg)		SFC: Specific Fuel Consumption, SFC = $\frac{\dot{m}_f}{P_{turb}}$	
e_f^* : Fuel Specific energy, (kWh/kg)		P_M : Electrical input power of the motor	
ξ : DoH in power, $\xi = \frac{P_b}{P_{total}}$		P_{MO}: Output power of the motor, $P_{MO} = \eta_M \cdot P_M$	
ψ : DoH in energy, $\psi = \frac{E_b}{E_{total}} = \frac{m_b \cdot e_b^*}{m_f \cdot e_f^* + mb \cdot e_b^*}$		P_{prop}: Propeller power, $P_{prop} = \eta_{prop} \cdot P_{shf}$	

Figure 3: Diagram of series hybrid electric propulsion

The range equation is calculated by the integral of cruise velocity over the total flying time,

$$R = \int_{t_i}^{t_f} V_\infty \cdot dt \tag{1}$$

The total installed energy variation over time is the combination of battery energy variation and fuel energy variation.

$$\frac{dE_{total}}{dt} = \frac{dE_f}{dt} + \frac{dE_b}{dt} \tag{2}$$

where, E_{total} is the total energy installed (kWh); E_f and E_b stand for the energy stored in fuel and batteries (kWh) respectively.

(i) Fuel Energy Change

The second term in Eq. 2 represents the rate of fuel energy variation. It is determined by the consumption rate of the fuel.

$$\frac{dE_f}{dt} = \frac{dm_f \times e_f^*}{dt} = e_f^* \frac{dm_f}{dt} = e_f^* \, \dot{m}_f \tag{3}$$

where, e_f^* represents the fuel specific energy density (kWh/kg) and $\dot{m}_f$ is the mass flow rate of fuel consumption (kg/s).

The efficiency of a combustion engine can be represented by the Specific Fuel Consumption (SFC). SFC is the mass flow of fuel consumed to provide shaft power. It is defined by dividing the fuel mass flow rate (kg/s) to the shaft output power (kW), SFC $= \dot{m}_f / P_{shf}$.

The rate of fuel energy variation hence can be also described as:

$$\frac{dE_f}{dt} = \frac{SFC \cdot P_{MG} \cdot e_f^*}{\eta_G} \tag{4}$$

where, P_{MG} is the power from engine generator to the motor; η_G is the energy conversion efficiency of the generator which transforms mechanical energy to electricity.

(ii) Battery Energy Change

The second term in Eq. 2 represents the variation of battery energy with time $\frac{dE_b}{dt}$; it can be calculated by the discharging rate. The battery weight is kept constant during the flight.

Degree-of-Hybridization (DoH) for Power

The electrical power transmitted to the motor P_M has two sources: batteries and electric generator, $P_M = P_{Mb} + P_{MG}$ as illustrated in Fig. 3. For a hybrid-electric propulsion, the ratio of electric power to the total installed power is declared as the parameter ξ, also called the Degree-of-Hybridization (DoH) for power [1]. It represents the percentage of maximum installed power in the total maximum installed power (motor, and fuel engine).

$$\xi = \frac{P_{Mb}}{P_M} \tag{5}$$

Combine Eq. 3 and 4 together with the DoH parameter ξ, we get

$$\frac{dE}{dt} = \mathbf{A} \cdot P_M \tag{6}$$

where, $\mathbf{A} = \left(\frac{e_f^* \cdot SFC \cdot (1-\xi)}{\eta_G} + \frac{\xi}{\eta_b}\right)$, represents the combined energy conversion efficiency with the consumption of fuel and battery power.

For a steady and level cruise flight with the velocity of V_∞, $L = W$, $T = D$. The propulsive power required by the aircraft is calculated by $P_{prop} = \frac{W \cdot V_\infty}{L/D}$. The propulsive power is obtained from the motor output power with

the propulsive efficiency $\eta_{prop} = \frac{P_{prop}}{P_{MO}}$; the motor output power is the product of total motor input power P_M and motor efficiency $\eta_M = \frac{P_{MO}}{P_M}$. Therefore, the motor input power can be obtained using the propulsive efficiency η_{prop} and motor efficiency η_M.

$$P_M = \frac{P_{MO}}{\eta_M} = \frac{P_{prop}}{\eta_M \cdot \eta_{prop}} = \frac{W \cdot V_\infty}{(L/D) \cdot \eta_{prop} \cdot \eta_M} \tag{7}$$

Therefore,

$$R = \int_{t_i}^{t_f} V_\infty dt = \int_{E_i}^{E_f} \frac{V_\infty}{\mathbf{A} \cdot P_M} \cdot dE = \frac{\eta_{prop} \cdot \eta_M}{\mathbf{A}} \cdot \frac{L}{D} \int_{E_i}^{E_f} \frac{1}{W}\, dE \tag{8}$$

Degree-of-Hybridization (DoH) for Energy

The ratio of stored electric energy to the total stored energy of the whole propulsion system is to describe the Degree-of-Hybridization (DoH) for energy [1],

$$\psi = \frac{E_b}{E} \tag{9}$$

where, the total energy is $E = E_f + E_b$.

Using above definition of DoH parameter ψ, the gross weight change is thus correlated with the total energy change,

$$dW = \frac{\psi e_f^* + (1-\psi) e_b^*}{e_f^*\, e_b^*}\, g\, dE = \frac{g}{\mathbf{B}}\, dE \tag{10}$$

where, $\mathbf{B} = \dfrac{e_f^*\, e_b^*}{\psi e_f^* + (1-\psi) e_b^*}$; it can be interpreted as an equivalent specific energy for the whole energy storage system.

Insert Eq. 10 into Eq. 8 and integrate this equation, we obtain the range equation for hybrid electric propulsion,

$$R = \frac{\mathbf{B} \cdot \eta_{prop} \cdot \eta_M}{\mathbf{A} \cdot g} \cdot \frac{L}{D} \cdot \ln\Big(\frac{W_i}{W_f}\Big) \tag{11}$$

3 CFJ Hybrid Electric Regional Airliner (CFJ-HERA)

The ATR72 families produced in France and Italy by aircraft manufacturer ATR are widely recognized as one of the most cost-effective regional airliner. The ATR72 has twin turbo-prop engines made to carry 72 passengers. It has a high wing configuration equipped with twin P&W 127F/M turbo-prop engines, designed for efficiency and operational flexibility. The isometric view and dimensions of ATR72 are shown in Fig. 4. The ATR72-500 variant is chosen as the baseline for comparison to evaluate the performance of the CFJ-HERA airplane.

3.1 CFJ Parameter Definitions

For CFJ flow control, the following parameter definitions are given to facilitate the explanation.

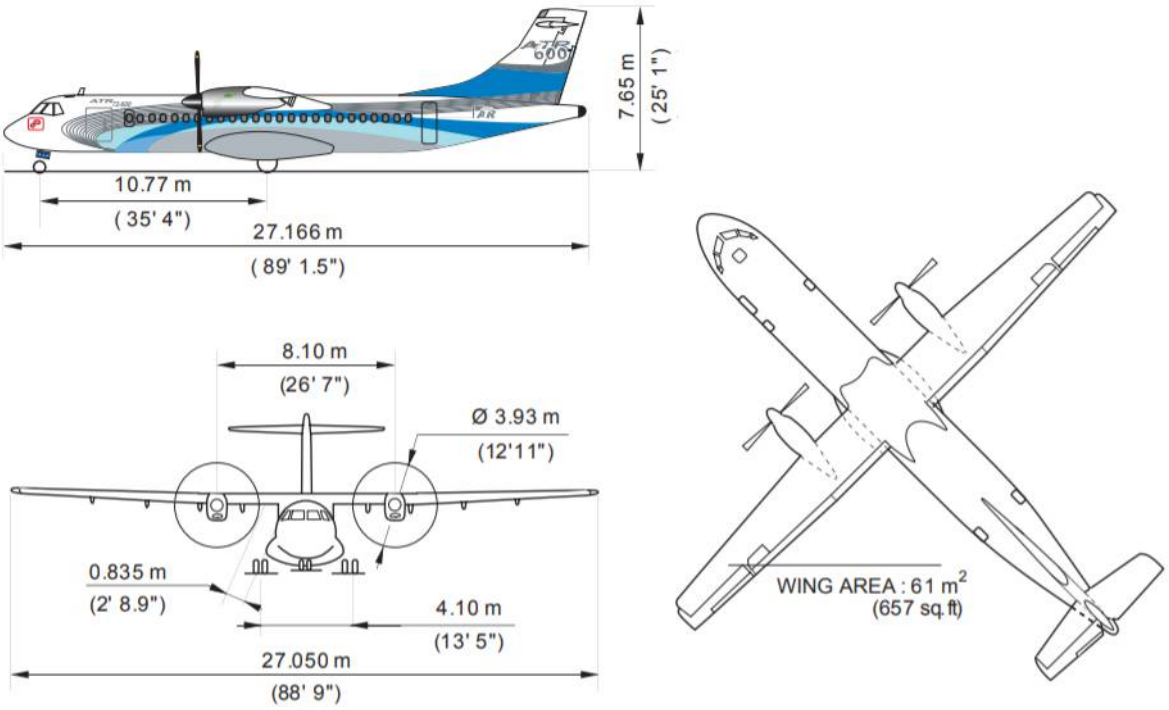

Figure 4: The isometric view and dimension of ATR72 regional airliner (Figure and dimensions are from [19]).

3.1.1 Jet Momentum Coefficient C_μ

The jet momentum coefficient C_μ is a parameter used to quantify the injection intensity. It is defined as :

$$C_\mu = \frac{\dot{m}V_j}{\frac{1}{2}\rho_\infty {V_\infty}^2 S} \tag{12}$$

where $\dot{m}$ is the injection mass flow, V_j the injection velocity, ρ_∞ and V_∞ denote the free stream density and velocity, and S is the platform area.

3.1.2 Power Coefficient P_c

The CFJ can be implemented by mounting a pumping system inside the wing that withdraws air from the suction slot and blows it into the injection slot. The power consumption can be determined by the jet mass flow and total enthalpy change as the following :

$$P = \dot{m}(H_{t1} - H_{t2}) \tag{13}$$

where H_{t1} and H_{t2} are the total enthalpy in the injection cavity and suction cavity respectively, P is the Power required by the pump and $\dot{m}$ the jet mass flow rate. Introducing the pumping efficiency η and total pressure ratio of the pump $\Gamma = \frac{P_{t1}}{P_{t2}}$, the power consumption can be expressed as :

$$P = \frac{\dot{m}C_pT_{t2}}{\eta}(\Gamma^{\frac{\gamma-1}{\gamma}} - 1) \tag{14}$$

The power consumption can be expressed as a power coefficient below:

$$P_c = \frac{P}{\frac{1}{2}\rho_\infty V_\infty^3 S} \tag{15}$$

In this research, the pumping efficiency of 100% is used for all the simulations unless indicated otherwise.

3.1.3 Corrected Aerodynamic Efficiency

The conventional airfoil aerodynamic efficiency is defined as $\frac{L}{D}$. However since CFJ active flow control consumes energy, the CFJ corrected aerodynamic efficiency is modified to take into account the energy consumption of the pump. The formulation of the corrected aerodynamic efficiency for CFJ airfoils is :

$$(\frac{L}{D})_c = \frac{L}{D + \frac{P}{V_\infty}} = \frac{C_L}{C_D + P_c} \tag{16}$$

where V_∞ is the free stream velocity, P is the CFJ pumping power, and L and D are the lift and drag generated by the CFJ airfoil. This formulation converts the power consumed by the CFJ into the drag of the airfoil. If the pumping power is set to 0, this formulation returns to the aerodynamic efficiency of a conventional airfoil.

3.1.4 Aircraft Productivity

To compare aircraft that have the same ratio of initial weight to final weight with the same engine fuel consumption or battery energy density, the productivity efficiency C_L^2/C_D is introduced to measure the productivity parameter [13].

The productivity efficiency $C_L^2/C_D = C_L(C_L/C_D)$ is a more comprehensive parameter than the conventional aerodynamic efficiency C_L/C_D to measure the merit of an airplane aerodynamic design for cruise performance. The former includes not only the information of C_L/C_D, but also the information of the aircraft weight C_L. For example, for two airplane designs having the same C_L/C_D with one C_L twice larger than the other, if the wing sizes are the same, one airplane will be able to carry twice more weight than the other with productivity and wing loading increased by 100%. Such a large difference is not reflected by C_L/C_D, but very well reflected by C_L^2/C_D.

For CFJ airfoil, the minimum CFJ pumping power occurs at a fairly high AoA [9, 11]. With the augmentation of CFJ, the subsonic cruise lift coefficient of a CFJ airfoil is typically 2 to 3 times higher than the conventional airfoil with about the same $(C_L/C_D)_c$ [20]. Such a high lift coefficient is unattainable for conventional airfoil since they would be either stalled or near stalled with very high drag. Hence for CFJ aircraft design, the productivity efficiency $C_L^2/C_D = C_L(C_L/C_D)$ is more informative to be used to reflect the aerodynamic performance. The corrected productivity efficiency for CFJ airfoils is

$$\frac{C_L^2}{C_D} = \frac{C_L^2}{C_D + P_c} \tag{17}$$

3.2 Design Requirement

The design objective of the CFJ regional airliner is to keep the same wing area of ATR72-500 and maximize the payload and range using CFJ wing and hybrid electric propulsion. The design includes sizing, CFJ wing, and

hybrid electric propulsion system. The original horizontal tail is enlarged to overcome the increased nose down pitching moment of CFJ wing. The sizing of fuselage is based on the original ATR72 scaled with the increased payload and passenger numbers.

An iterative procedure to determine the maximum takeoff weight of the CFJ-HERA aircraft based on Eq. (11) is developed. A comparison of mission parameters of the CFJ-HERA and ATR72-500 is summarized in Table 1. We choose two aspect ratios of 12 and 20 for the wing of CFJ-HERA airplane. A significant performance improvement is achieved for CFJ-HERA aircraft. The major advantage of CFJ aircraft is its ultra-high productivity efficiency with high cruise lift coefficient. The CFJ-HERA-AR12 and ATR72-500 have the same wing configuration (chord, span, area, and aspect ratio). The CFJ-HERA-AR12 achieves a productivity efficiency of 21.3, substantially higher than the productivity efficiency of 15.3 for ATR72-500. Further improvement is obtained in CFJ-HERA-AR20, which has the same wing area with a higher aspect ratio of 20. The productivity efficiency for CFJ-HERA-AR20 is 29.3, an increase of 91% compared with that of ATR72-500.

The wing loading for CFJ wings is substantially increased for the CFJ-HERA airplanes. Therefore, the maximum takeoff weight is increased from 22800 kg and 45620 kg for CFJ-HERA-AR20. The maximum fuel weight is increased to 18400 kg with the battery weight of 8090 kg attributed to the high wing loading. The larger amount of fuel and batteries allows the airliner to fly a much longer range. The conceptual CFJ wing design with embeded CFJ compressor of the CFJ-HERA regional airliner is depicted in Fig. 5.

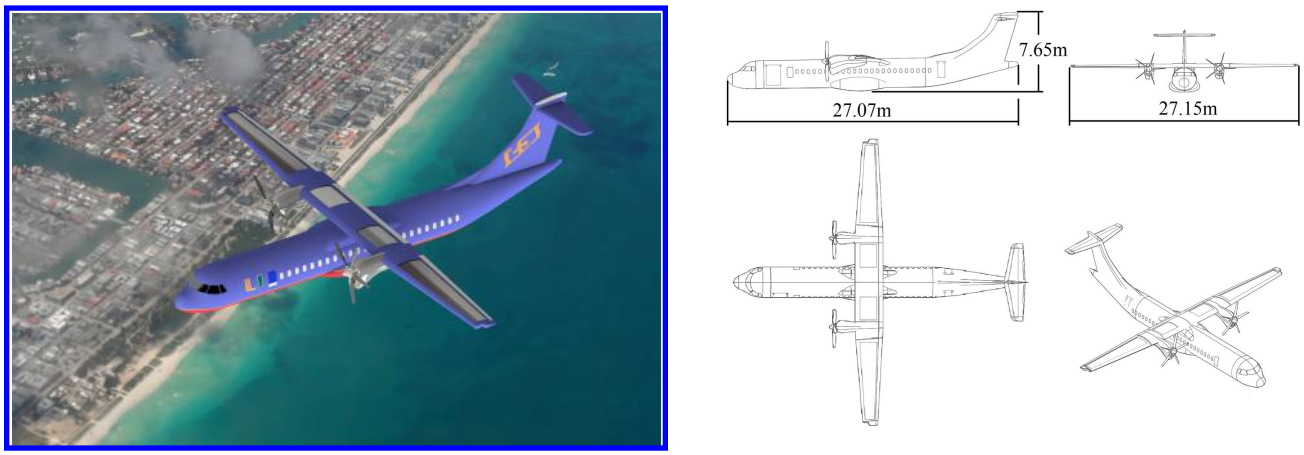

Figure 5: CFJ-HERA regional airliner.

The weight decomposition of the conventional turboprop airliner and CFJ hybrid electric airliner is illustrated in Fig. 6. With reference to the maximum takeoff weight (MTOW) of the conventional airliner, the total weight of a CFJ aircraft is substantially increased because of the high lift coefficient and wing loading of the CFJ wing in order to extend the range. The hybrid electric airliner needs to carry a certain amount of batteries as a secondary energy storage. The turbo engines always operate at the optimal efficiency point to drive the propulsor and charge the battery during cruise. Extra weight is introduced by the modified powertrain system with additional components. The energy distribution of fuel and batteries is controlled by the energy split factor $\psi = 0.01$ and power split factor $\xi = 0.01$.

Table 1: Comparison of mission performances for CFJ-HERA and ATR72-500

Parameters	ATR72-500	CFJ-HERA-AR12	CFJ-HERA-AR20	Unit
Maximum Take-off Weight (MTOW)	22800	40460	45620	kg
Range	890	1,960	2,850	nm
Maximum payload weight	7200	7200	7200	kg
Maximum fuel weight	5000	14800	18400	kg
Battery weight	-	6460	8090	kg
Wing surface	61.25	61.25	61.25	m^2
Wing span	27.15	27.15	35	m
Aspect ratio	12	12	20	-
Wing loading	369	660	746	m/s
Cruise Mach	0.46	0.46	0.46	-
Aircraft Aerodynamic efficiency	23.9	18.4	22.4	-
Aircraft Productivity efficiency	15.3	21.3	29.3	-

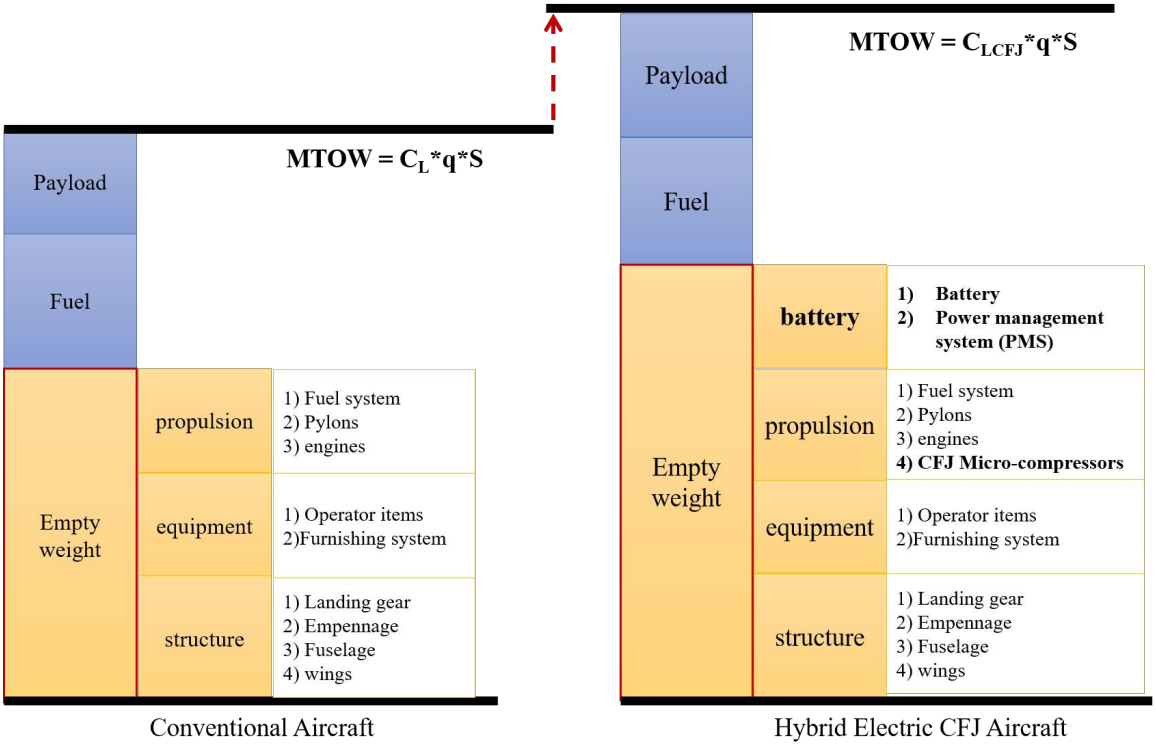

Figure 6: The weight decomposition of a conventional and CFJ airliner with hybrid electric propulsion

3.3 Propulsion System

The hybrid electric propulsion is different from the conventional propulsion system in its electric power transmission system. In a conventional propulsion system, the integrated engines and propulsors directly convert chemical energy to mechanical energy. For a hybrid electric propulsion system, the gas combustor, turbines, generators, and electric motors are separated components. For a series hybrid electric propulsion, the first step is to convert chemical energy of kerosene into electricity. The combustor, turbine, and generator are required for this process.

A power management system (PMS) is needed to control the electricity source, storage, distribution, and consumption. It also ensures safe operation by controlling the voltage and current level. The electric motors convert the electric energy into the shaft power, then drive the propeller.

The power chain requirement is given in Table 2. The power requirement calculation follows the reverse direction in Fig. 3. The thrust during the cruise of the whole aircraft is 14003.26 N. The power requirement for the propeller can be calculated by the cruise speed and thrust forces with the propeller efficiency. The motor power is obtained followed by the shaft power calculation. With the known motor power, the weight decomposition of electric components can be analyzed as shown in Table 3. The total weight of the electrical components is 693.7 kg. The fuel and battries weight are listed in Table. 4.

Table 2: Power chains of propulsion components for CFJ-HERA

Components	Power requirement	unit	Efficiency
Thrust	14003.26	N	-
Propeller power	1995.24	KW	0.8
shaft power	2494.05	kW	0.95
motor power	2625.31	kW	0.95
CFJ compressor	512.26	kW	0.7

Table 3: Weight decomposition of propulsion components for CFJ-HERA

Components	Gravimetric Density (kW/kg)	Efficiency	Weight(kg)
Electric motor	15	0.95	175.0
Inverter/converter	20	0.98	131.3
Electric cable	20	0.985	131.2
CFJ compressor	2	0.7	256.1
Total	-	-	693.7

Table 4: Fuel and battery weight for CFJ-HERA

-	Fuel	Battery
Specific Energy (kWh/kg)	11.6	0.26
Conversion efficiency	35%	95%
Weight for AR12 (kg)	14800	6460
Weight for AR20 (kg)	18400	8090

* DoH for power $\xi = 0.01$ and DoH for energy $\psi = 0.01$

3.4 CFJ Wing Design

The CFJ6421-SST150-SUC247-INJ117 airfoil is used for the current CFJ-HERA design. A trade study was performed by Wang and Zha [21]. The current CFJ airfoil has an enlarged injection slot size and suction slot size compared with the one used in [10] to substantially reduce the CFJ power consumption. And the suction slot angle is adjusted to achieve drag reduction. The CFJ-HERA wing with micro-compressors is shown in Fig. 7. The CFJ-HERA wing has a wing area of 61 m^2.

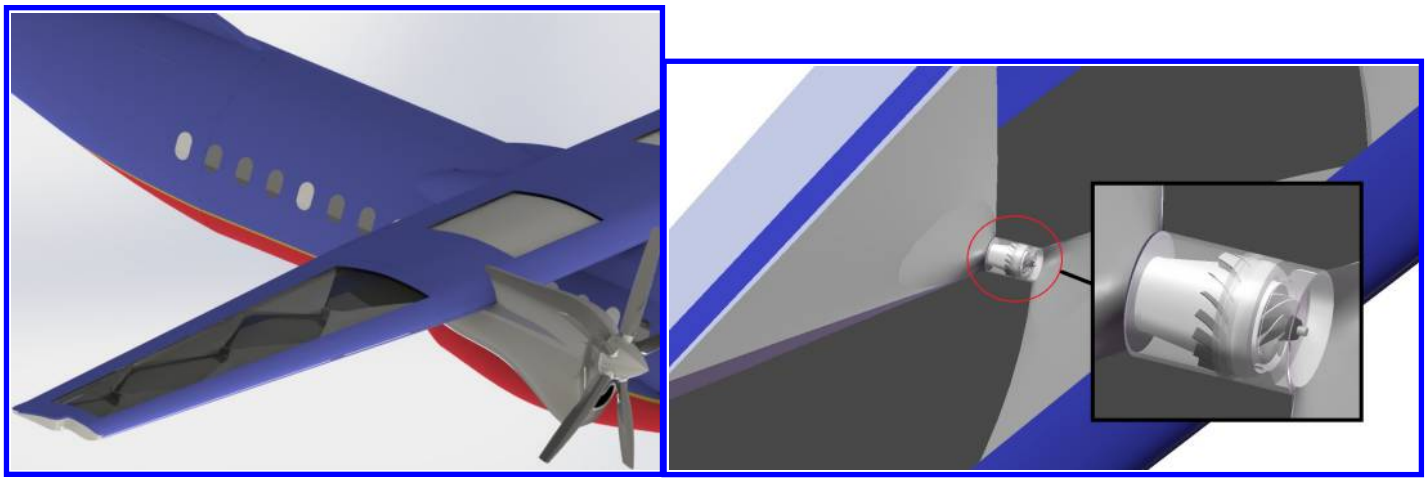

Figure 7: CFJ-HERA wing configuration with micro-compressors

3.5 Cruise Performance

Table 5: CFJ-HERA wing cruise parameters for AR = 12 and AR = 20.

Case	AR	Mach	AoA	Cμ	C_L	C_D	P_c	C_L/C_D	C_L/C_{Dc}	C_L^2/C_{Dc}
AR12 cruise	12	0.46	4	0.02	1.158	0.042	0.0079	27.6	23.2	26.9
AR20 cruise	20	0.46	5	0.02	1.31	0.039	0.007	34	28.8	37.7

The CFJ-HERA airliner cruises at the speed of Mach number of 0.46 at the altitude of 7600 m. A RANS simulation of the 3D CFJ wing is conducted for the cruise condition with the Reynolds number of 3.0 million. A trade study for the best efficiency point is conducted with various angle of attack and jet momentum coefficient. Table 5 shows the aerodynamic parameters for the CFJ wings. As a reference, the aerodynamic efficiency for the baseline ATR72-500 is 23.9 and the productivity efficiency is 15.3. For CFJ-HERA-AR12 (left plot of Fig. 8), the peak efficiency point is observed at the AoA of 4° and C_μ of 0.02. The lift coefficient is 1.158 and drag coefficient is 0.04. The corrected aerodynamic efficiency L/D_c of 23.2 and productivity efficiency C_L/C_{Dc} of 26.9 is achieved. For CFJ-HERA-AR20 (right plot of Fig. 8), both the aerodynamic efficiency and productivity efficiency are significantly improved with the larger aspect ratio of 20. The peak aerodynamic efficiency of 28.8 and productivity efficiency of 37.7 is obtained at AoA of 5° and C_μ of 0.02. The lift coefficient is increased to 1.31 at this peak efficiency point. As shown above, the CFJ-HERA wing design has a significant improvement in the aerodynamic efficiency and productivity efficiency. In comparison with the baseline ATR72-500, the productivity efficiency for the CFJ-HERA-AR20 is increased by 146% using the same wing area.

4 Conclusions

This paper investigates the potential benefits of Co-Flow jet (CFJ) hybrid electric propulsion (HEP) aircraft through a conceptual design of a regional airliner. The ATR72-500 regional airliner is chosen as a reference. The ATR72-500 aircraft has a range of 890 nm, a payload of 72 passengers and cruise Mach number of 0.46. The mission of the current CFJ hybrid electric regional airliner (CFJ-HERA) is to extend the range of ATR72-500. The CFJ-HERA uses an optimized CFJ wing configuration based on the CFJ6421-SST150-INJ117-SUC247 airfoil. Two different aspect ratios of 12 and 20 are studied for comparison. Both achieve substantially higher

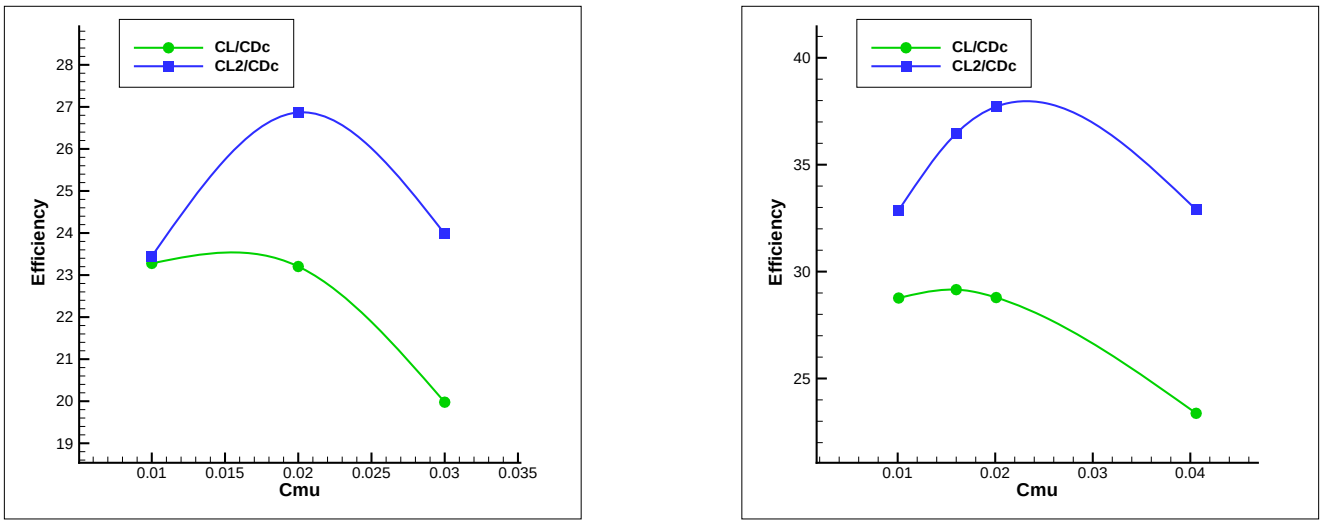

CFJ-HERA-AR12, AoA = 4° CFJ-HERA-AR20, AoA = 5°

Figure 8: Corrected aerodynamic efficiency L/D_c and productivity efficiency C_L/C_{Dc} vesus C_μ.

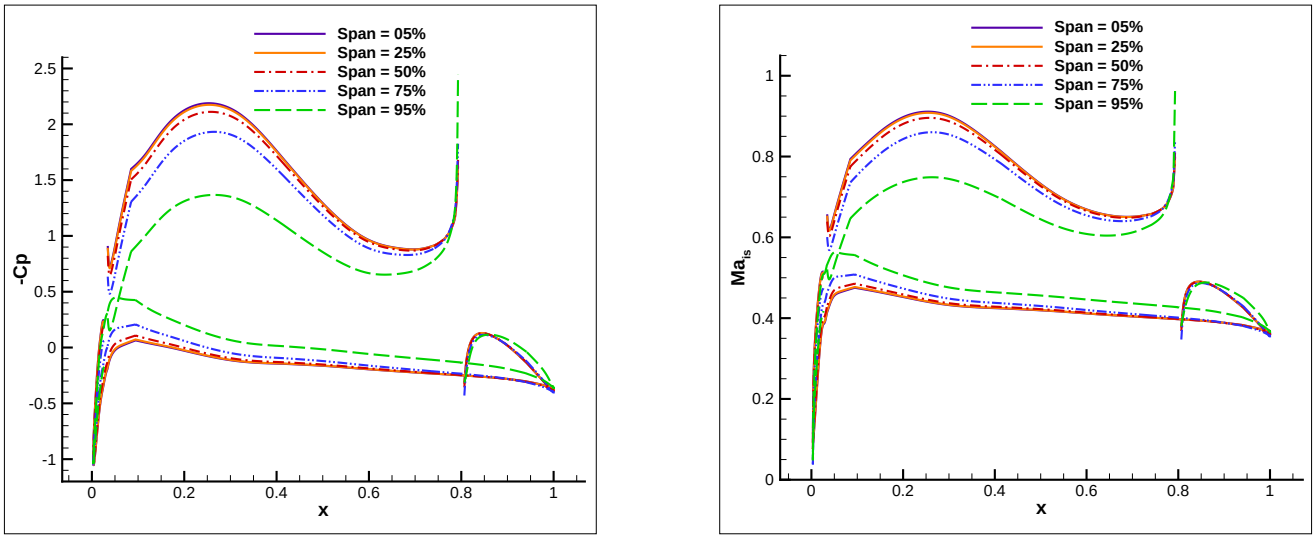

Figure 9: Pressure coefficient C_p and isentropic Mach number Ma_{is} of the CFJ-HERA-AR12 wing at AoA of 4° and C_μ of 0.02.

productivity efficiency than the baseline ATR72-500 airliner. With the same wing area as that of ATR72-500, the CFJ-HERA-AR12 design achieves a substantially longer range of 1960 nm and the CFJ-HERA-AR20 further extends the range to 2850 nm. Due to the high lift cruise coefficient of CFJ wing, the CFJ-HERA has a wing loading of 660 kg/m^2 and 746 kg/m^2 for AR of 12 and 20 respectively. In addition to the increased productivity efficiency, the significantly higher wing loading allows the airliner to carry much more fuel and batteries without increasing the wing size and weight, which contributes to the substantially longer range. The conceptual design of the CFJ-HERA indicates that the CFJ technology has a great potential to contribute the development of hybrid propulsion aircraft.

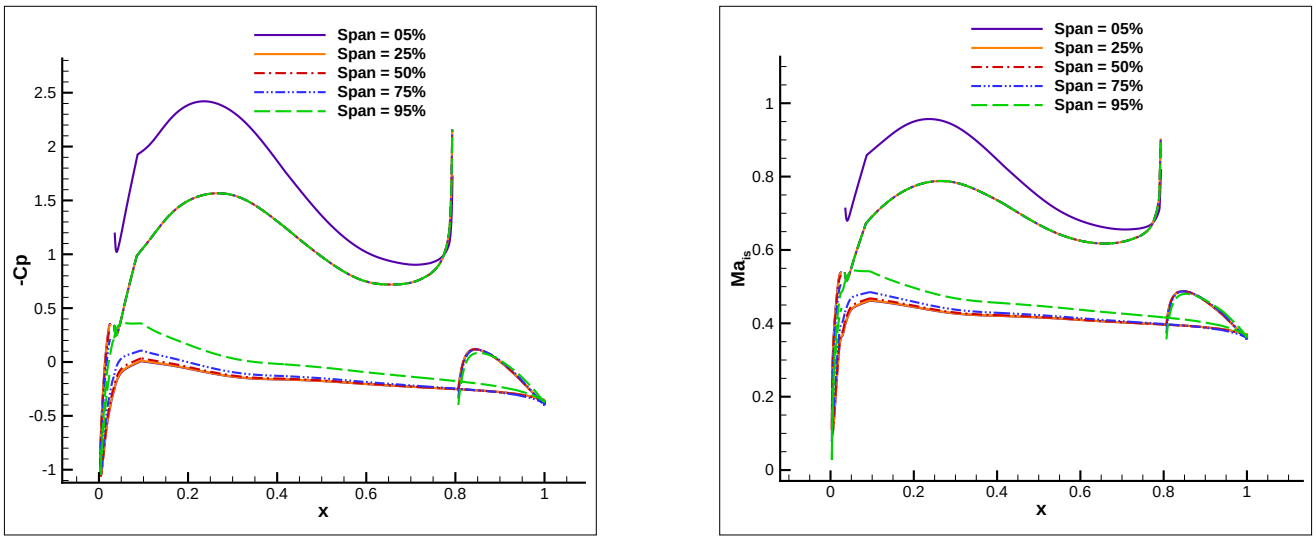

Figure 10: Pressure coefficient C_p and isentropic Mach number Ma_{is} of the CFJ-HERA-AR20 wing at AoA of 5° and C_μ of 0.02.

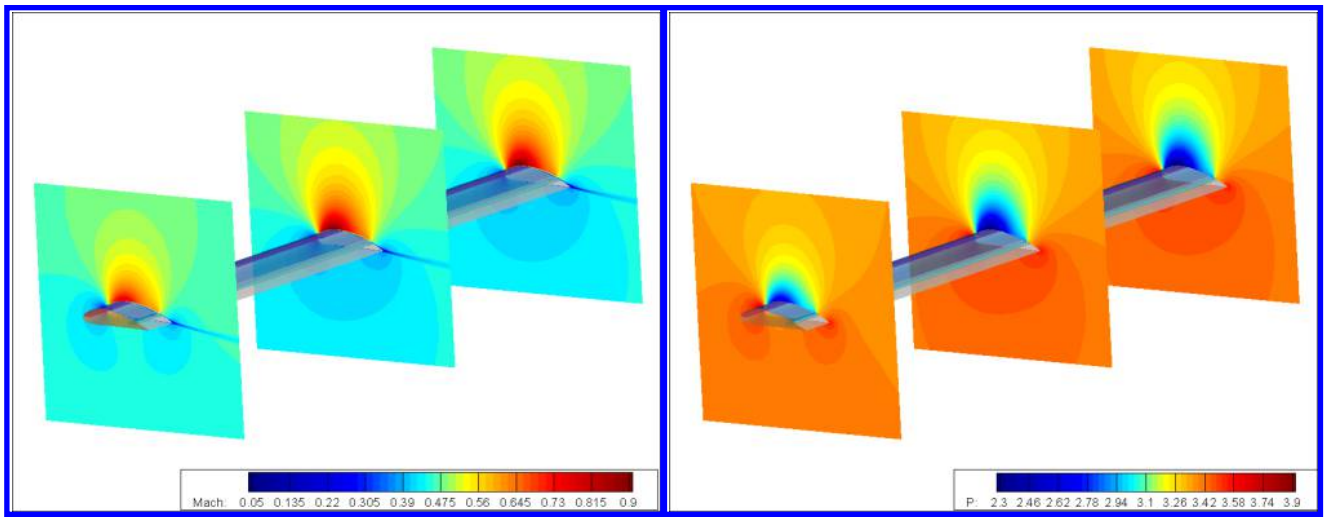

Figure 11: The Mach number and pressure contour of the CFJ-HERA-AR20 wing

5 Acknowledgment

The simulations was conducted on Pegasus supercomputing system at the Center for Computational Sciences at the University of Miami.

APPENDIX
Range Equation for Hybrid Electric Propulsion

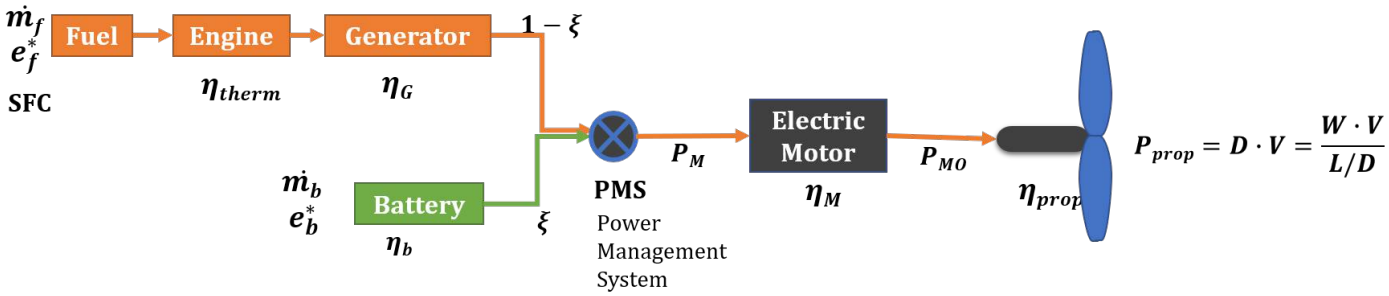

E_{total} : Total installed energy, (kWh)		η_{therm} :	Efficiency of the combustion engine;
E_b :	Battery installed energy, (kWh)	η_b :	Battery charging and discharging efficiency;
m_b :	Battery weight, (kg)	η_M :	Efficiency of the electric motor;
m_f :	Fuel weight, (kg)	η_{prop} :	Propeller efficiency;
e_b^* :	Battery Specific energy, (kWh/kg)	SFC:	Specific Fuel Consumption, SFC = $\frac{\dot{m}_f}{P_{turb}}$
e_f^* :	Fuel Specific energy, (kWh/kg)	P_M :	Electrical input power of the motor
ξ :	DoH in power, $\xi = \frac{P_b}{P_{total}}$	P_{MO}:	Output power of the motor, $P_{MO} = \eta_M \cdot P_M$
ψ :	DoH in energy, $\psi = \frac{E_b}{E_{total}} = \frac{m_b \cdot e_b^*}{m_f \cdot e_f^* + mb \cdot e_b^*}$	P_{prop}:	Propeller power, $P_{prop} = \eta_{prop} \cdot P_{shf}$

Figure 12: Diagram of series hybrid electric propulsion

The range equation is calculated by the integral of cruise velocity over time,

$$R = \int_{t_i}^{t_f} V_\infty dt \tag{18}$$

The total installed energy variation over time is the combination of battery energy variation and fuel energy variation.

$$\frac{dE_{total}}{dt} = \frac{dE_f + dE_b}{dt} = \frac{dE_f}{dt} + \frac{dE_b}{dt} \tag{19}$$

where, E_{total} is the total energy installed (kWh); E_f and E_b represent the energy stored in fuel form and in batteries (kWh) respectively.

Fuel Energy Variation

The rate of fuel energy over time is determined by the fuel weight variation.

$$\frac{dE_f}{dt} = \frac{dm_f \times e_f^*}{dt} = e_f^* \frac{dm_f}{dt} = e_f^* \, \dot{m}_f \tag{20}$$

where, e^* represents specific energy density (kWh/kg) and $\dot{m}_f$ is the mass flow rate of fuel consumption (kg/s).

The fuel efficiency of an engine can be represented by the Specific Fuel Consumption (SFC). SFC is the mass flow of fuel needed to provide the net thrust or shaft power. It is defined by dividing the fuel mass flow rate (kg/s) to the shaft output power (kW),

$$\mathrm{SFC} = \frac{\dot{m}_f}{P_{shf}} \tag{21}$$

Insert SFC definition into the dE_f Eqn. 20,

$$\frac{dE_f}{dt} = \mathrm{SFC} \cdot P_{shf} \cdot e_f^* \tag{22}$$

$\frac{dE_f}{dt}$ can also be described using the energy conversion efficiency chains,

$$P_{shf} = e_f^* \cdot \dot{m}_f \cdot \eta_t \tag{23}$$

where, η_{therm} is the thermal efficiency of the engine.

Then, the power output from the generator can be described as

$$P_{MG} = P_{shf} \cdot \eta_G \tag{24}$$

where, η_G is the energy conversion efficiency of the generator from the input shaft power to electric power output.

Therefore, the rate of fuel energy variation rate derived as,

$$\frac{dE_f}{dt} = \frac{SFC \cdot P_{MG} \cdot e_f^*}{\eta_G} \tag{25}$$

Battery Energy Variation

The second term in Eq. 19 represents the change of battery energy with time $\frac{dE_b}{dt}$; it can be calculated by

$$\frac{dE_b}{dt} = \mathrm{const} \tag{26}$$

Here, we assume that the battery discharge rate is constant. The weight of battery remains basically unchanging.

Electrical Power

The electrical power transmitted to the motor P_M has two sources: batteries and electric generator,

$$P_M = P_{Mb} + P_{MG} \tag{27}$$

For a hybrid-electric propulsion, the ratio of electric power to the total installed power is declared as the parameter ξ, also called as the Degree-of-Hybridization (DoH) for power [1]. It represents the percentage of maximum installed electric power in the total maximum installed power (motor, and fuel engine).

$$\xi = \frac{P_{Mb}}{P_M} \tag{28}$$

Then, the rate of variation of battery installed energy is represented as,

$$\frac{dE_b}{dt} = \frac{P_{Mb}}{\eta_b} = \frac{P_M \ \xi}{\eta_b} \tag{29}$$

where η_b is the battery energy conversion efficiency.

Combine Eq. (22) and (29), we get

$$\frac{dE}{dt} = SFC \cdot P_{MG} \cdot e_f^* + \frac{P_{Mb}}{\eta_b} = P_M \left(\frac{e_f^* \cdot SFC \cdot (1-\xi)}{\eta_G} + \frac{\xi}{\eta_b} \right) \tag{30}$$

To simplify the above formula,

$$\frac{dE}{dt} = \mathbf{A} \cdot P_M \tag{31}$$

where, $\mathbf{A} = \left(\frac{e_f^* \cdot SFC \cdot (1-\xi)}{\eta_G} + \frac{\xi}{\eta_b} \right)$, represents the combined energy conversion efficiency with the consumption of fuel and battery power.

$$dt = \frac{dE}{\mathbf{A} \cdot P_M} \tag{32}$$

For a steady and level cruise flight with the velocity of V_∞, $L = W$, $T = D$. The propulsive power required by the aircraft is calculated by

$$P_{prop} = T \cdot V_\infty = D \cdot V_\infty = \frac{W \cdot V_\infty}{L/D} \tag{33}$$

The propulsive power is obtained from the motor output power with the propulsive efficiency $\eta_{prop} = \frac{P_{prop}}{P_{MO}}$; the motor output power is the product of total motor input power P_M and motor efficiency $\eta_M = \frac{P_{MO}}{P_M}$. Therefore, the motor input power can be obtained using the propulsive efficiency η_{prop} and motor efficiency η_M.

$$P_M = \frac{P_{MO}}{\eta_M} = \frac{P_{prop}}{\eta_M \cdot \eta_{prop}} = \frac{W \cdot V_\infty}{(L/D) \cdot \eta_{prop} \cdot \eta_M} \tag{34}$$

Therefore,

$$R = \int_{t_i}^{t_f} V_\infty dt = \int_{E_i}^{E_f} \frac{V_\infty}{\mathbf{A} \cdot P_M} \cdot dE = \int_{E_i}^{E_f} \frac{\eta_{prop} \cdot \eta_M}{\mathbf{A} \cdot W} \cdot \frac{L}{D} \, dE \tag{35}$$

$$R = \frac{\eta_{prop} \cdot \eta_M}{\mathbf{A}} \cdot \frac{L}{D} \int_{E_i}^{E_f} \frac{1}{W} \, dE \tag{36}$$

The overall aircraft weight consists of the four contributions: empty weight, payload weight, fuel weight, and battery weight,

$$W = W_{empty} + W_{payload} + W_f + W_b \tag{37}$$

The total stored energy of the whole propulsion system E is the sum of electric energy and fuel energy,

$$E = E_f + E_b = e_f^* \, m_f + e_b^* \, m_b \tag{38}$$

The ratio of stored electric energy to the total stored energy of the whole propulsion system is to describe the Degree-of-Hybridization (DoH) for energy [1],

$$\psi = \frac{E_b}{E} = \frac{e_b^* \, m_b}{e_f^* \, m_f + e_b^* \, m_b} \tag{39}$$

$$W_f + W_b = (m_f + m_b)g = (\frac{E(1-\psi)}{e_f^*} + \frac{E\psi}{e_b^*})g = \frac{\psi e_f^* + (1-\psi)e_b^*}{e_f^* \, e_b^*} gE \tag{40}$$

$$W = \frac{\psi e_f^* + (1-\psi)e_b^*}{e_f^* \, e_b^*} gE + W_{structure} + W_{payload} \tag{41}$$

The change of aircraft gross weight is thus correlated with the total energy change,

$$dW = \frac{\psi e_f^* + (1-\psi)e_b^*}{e_f^* \, e_b^*} \, g \, dE = \frac{g}{\mathbf{B}} \, dE \tag{42}$$

where, $\mathbf{B} = \dfrac{e_f^* \, e_b^*}{\psi e_f^* + (1-\psi)e_b^*}$, it can be interpreted as an equivalent specific energy for the whole energy storage system.

Insert Eq. 42 into Eq. 36 and integrate this equation, we obtain the range equation for hybrid electric propulsion,

$$R = \frac{\mathbf{B} \cdot \eta_{prop} \cdot \eta_M}{\mathbf{A} \cdot g} \cdot \frac{L}{D} \cdot \ln\Big(\frac{W_i}{W_f}\Big) \tag{43}$$

For the pure fuel case, If $\psi = 0$, then $\mathbf{B} = e_f^*$; If $\xi = 0$, then $\mathbf{A} = \frac{e_f^* \cdot SFC}{\eta_g}$, If we assume that $\eta_G = 100\%$, $\eta_M = 100\%$. the range equation is reduced to

$$R = \frac{\eta_{prop}}{SFC \cdot g} \cdot \frac{L}{D} \cdot \ln\Big(\frac{W_i}{W_f}\Big) \tag{44}$$

which is exactly the same as Bregruet range equation.

References

[1] C. Pornet and A. Isikveren, "Conceptual Design of Hybrid-electric Transport Aircraft," *Progress in Aerospace Sciences*, vol. 79, no. Supplement C, pp. 114 – 135, 2015.

[2] J. L. Felder, G. V. Brown, H. DaeKim, and J. Chu, "Turboelectric Distributed Propulsion in a Hybrid Wing Body Aircraft." 20th International Society for Airbreathing Engines (ISABE 2011), 2011.

[3] G.-C. Zha, W. Gao, and C. Paxton, "Jet Effects on Co-flow Jet Airfoil Performance," *AIAA Journal, No. 6,*, vol. 45, pp. 1222–1231, 2007.

[4] G.-C. Zha and D. C. Paxton, "A Novel Flow Control Method for Airfoil Performance Enhancement Using Co-flow Jet." *Applications of Circulation Control Technologies*, Chapter 10, p. 293-314, Vol. 214, Progress in Astronautics and Aeronautics, AIAA Book Series, Editors: Joslin, R. D. and Jones, G.S., 2006.

[5] G.-C. Zha, C. Paxton, A. Conley, A. Wells, and B. Carroll, "Effect of Injection Slot Size on High Performance Co-flow Jet Airfoil," *AIAA Journal of Aircraft*, vol. 43, 2006.

[6] G.-C. Zha, B. Carroll, C. Paxton, A. Conley, and A. Wells, "High Performance Airfoil With Co-flow Jet Flow Control," *AIAA Journal*, vol. 45, pp. 2087–2090, 2007.

[7] Wang, B.-Y. and Haddoukessouni, B. and Levy, J. and Zha, G.-C., "Numerical Investigations of Injection Slot Size Effect on the Performance of Co-flow Jet Airfoil ," *AIAA Journal of Aircraft*, vol. 45, pp. 2084–2091, 2008.

[8] B. P. E. Dano, D. Kirk, and G.-C. Zha, "Experimental Investigation of Jet Mixing Mechanism of Co- Flow Jet Airfoil." AIAA-2010-4421, 5th AIAA Flow Control Conference, Chicago, IL, 28 Jun - 1 Jul 2010.

[9] B. P. E. Dano, G.-C. Zha, and M. Castillo, "Experimental Study of Co-flow Jet Airfoil Performance Enhancement Using Micro Discreet Jets." 49th AIAA Aerospace Sciences Meeting, AIAA-2011-0941, 2011.

[10] Lefebvre, A. and Zha, G.-C. , "Design of High Wing Loading Compact Electric Airplane Utilizing Co-flow Jet Flow Control." 53rd AIAA Aerospace Sciences Meeting, AIAA SciTech Forum, (AIAA 2015-0772), 2015.

[11] Lefebvre, A. and Dano, B. and Bartow, W. and Di Franzo, M. and Zha, G.-C., "Performance Enhancement and Energy Expenditure of Co-flow Jet Airfoil With Variation of Mach Number," *Journal of Aircraft*, no. 6, pp. 1757–1767, 2016.

[12] Liu, Z.-X. and Zha, G.-C., "Transonic Airfoil Performance Enhancement Using Co-flow Jet Active Flow Control." AIAA Paper 2016-3066, AIAA Aviation, 2016.

[13] Y. Yang and G. Zha, "Super-lift Coefficient of Active Flow Control Airfoil: What Is the Limit?." 55th AIAA Aerospace Science Meeting, AIAA Paper 2017-1693, 2017.

[14] Y. Yang and G. Zha, "Numerical Simulation of Super-Lift Coefficient of Co-Flow Jet Flow Control Wing." 2018 AIAA Aerospace Sciences Meeting, AIAA SciTech Forum, (AIAA 2018-2054),Kissimmee, Florida, 2018.

[15] Y. Yang and G. Zha, "Super Lift Coefficient of Co-Flow Jet Circular Cylinder." 2018 AIAA Aerospace Sciences Meeting, AIAA SciTech Forum, (AIAA 2018-0329),Kissimmee, Florida, 2018.

[16] Y. Yang and G. Zha, "Improved Delayed Detached Eddy Simulation of Super-Lift Coefficient of Subsonic Co-Flow Jet Flow Control Airfoil." 2018 AIAA Aerospace Sciences Meeting, AIAA SciTech Forum, (AIAA 2018-0314)Kissimmee, Florida, 2018.

[17] Y. Yang and G.-C. Zha, "Numerical Investigation of Performance Improvement of the Co-Flow Jet Electric Airplane." AIAA Aviation paper 2018, 2018.

[18] G.-C. Zha, Y. Yang, Y. Ren, B. Mcbreen, and E. White, "Wind Tunnel Testing of Super-Lifting and Thrusting CFJ Airfoil Actuated by Micro-Compressors." AIAA Paper-2018-3061, AIAA AVIATION Forum 2018, 2018 Flow Control Conference, June 25-29, 2018, Atlanta, Georgia, 2018.

[19] A. aircraft, "ATR Family Booklet," 2014.

[20] Lefebvre, A. and Zha, G.-C., "Trade Study of 3d Co-flow Jet Wing for Cruise Performance." 54th AIAA Aerospace Sciences Meeting, AIAA SciTech Forum, (AIAA 2016-0570), 2016.

[21] Y. Wang and G.-C. Zha, "Study of 3D Co-ow Jet Wing Induced Drag and Power Consumption at Cruise Conditions." AIAA SciTech 2019, 7-11 January 2019, Manchester Grand Hyatt San Diego, San Diego, California.

AIAA SciTech Forum
7-11 January 2019, San Diego, California
AIAA Scitech 2019 Forum

10.2514/6.2019-1584.c1

Correction: [Conceptual Design of a Co-Flow Jet Hybrid Electric Regional Airliner], AIAA Paper- 2019-1584

Author(s) Name: Yunchao Yang, Gecheng Zha
Author(s) Affiliations: University of Miami, Coral Gables, Florida 33124

Correction Notice:

The drag calculation of the baseline ATR72-500 was under-estimated by mis-calculating the fuselage drag. The performance of the baseline ATR72-500 was hence over-estimated. The corrected values of the aerodynamic efficiency and productivity efficiency of ATR72-500 are updated in Table 1 below. Specifically, in the Table 1 of the original paper, the ATR72-500 aerodynamic efficiency of 23.9 should be corrected to 15.95. The ATR72-500 productivity efficiency of 15.3 should be corrected to 10.2. The ATR72-500 baseline wing performance is also added in Table 5 below.

Subsequently, on page 9, 2nd paragraph, in the last three sentence from the end, the "the productivity efficiency of 15.3" should be changed to "the productivity efficiency of 10.2". In the same paragraph, in the last sentence, the "an increase of 91%" should be changed to "an increase of 187%".

Table 1: Comparison of mission performances for CFJ-HERA and ATR72-500

Parameters	ATR72-500	CFJ-HERA-AR12	CFJ-HERA-AR20	Unit
Maximum Take-off Weight (MTOW)	22800	40460	45620	kg
Range	890	1,960	2,850	nm
Maximum payload weight	7200	7200	7200	kg
Maximum fuel weight	5000	14800	18400	kg
Battery weight	-	6460	8090	kg
Wing surface	61.25	61.25	61.25	m^2
Wing span	27.15	27.15	35	m
Aspect ratio	12	12	20	-
Wing loading	369	660	746	m/s
Cruise Mach	0.46	0.46	0.46	-
Aircraft Aerodynamic efficiency	15.95	18.4	22.4	-
Aircraft Productivity efficiency	10.2	21.3	29.3	-

Table 5: CFJ-HERA wing cruise parameters for AR = 12 and AR = 20.

Case	AR	Mach	AoA	Cμ	C_L	C_D	P_c	C_L/C_D	C_L/C_{Dc}	C_L^2/C_{Dc}
baseline	12	0.46	4	-	0.64	0.027	-	23.7	23.7	15.1
AR12 cruise	12	0.46	4	0.02	1.158	0.042	0.0079	27.6	23.2	26.9
AR20 cruise	20	0.46	5	0.02	1.31	0.039	0.007	34	28.8	37.7